Jinlida granules alleviate podocyte apoptosis and mitochondrial dysfunction via the AMPK/PGC-1α pathway in diabetic nephropathy

SHENGNAN SUN*, SHURONG YANG*, YING CHENG*, TING FANG, JINGRU QU, LEI TIAN, MAN ZHANG, SHI WU, BEI SUN and LIMING CHEN

NHC Key Laboratory of Hormones and Development, Tianjin Key Laboratory of Metabolic Diseases, Chu Hsien-I Memorial Hospital and Tianjin Institute of Endocrinology, Tianjin Medical University, Tianjin 300134, P.R. China

Received August 31, 2024; Accepted November 20, 2024

DOI: 10.3892/ijmm.2024.5467

Abstract. Traditional Chinese Medicine (TCM) has demonstrated promising efficacy in managing and preventing the early-stage diabetic nephropathy (DN). Although the exact mechanisms remain elusive, clinical evidence has suggested that Jinlida granules (JLD) are beneficial in improving renal function among patients with DN. The present study aimed to elucidate the effect of JLD on DN and the underlying molecular mechanism. Therefore, podocyte apoptosis was evaluated using flow cytometry and TUNEL staining, while mitochondrial morphology and function were assessed using transmission electron microscopy, MitoTracker, JC-1 and reactive oxygen species staining. RNA sequencing analysis was performed to elucidate the mechanism underlying the effect of JLD on DN. Additionally, to investigate the role of peroxisome proliferator-activated receptor-γ co-activator-1α (PGC-1α) in mitigating JLD-induced mitochondrial dysfunction and podocyte apoptosis, MPC5 cells were transfected with the corresponding small interfering RNA constructs. The results showed that JLD effectively improved renal function and mitigated podocyte injury, as well as ameliorated mitochondrial dysfunction and inhibited apoptosis in db/db mice. *In vitro* experiments further revealed that JLD exerted a protective effect via inhibiting mitochondrial fission and apoptosis in high glucose-treated podocytes. Furthermore, JLD enhanced the phosphorylation of adenosine monophosphate-activated protein kinase (AMPK), thus promoting the expression of PGC-1α, eventually improving apoptosis and mitochondrial homeostasis. Overall, the current study revealed that JLD could improve mitochondrial homeostasis and reduce cell apoptosis in podocytes via activating the AMPK/PGC-1α pathway, thus providing a theoretical foundation for the clinical management of DN.

Correspondence to: Professor Liming Chen or Dr Bei Sun, NHC Key Laboratory of Hormones and Development, Tianjin Key Laboratory of Metabolic Diseases, Chu Hsien-I Memorial Hospital and Tianjin Institute of Endocrinology, Tianjin Medical University, 6 Huanrui North Road, Beichen, Tianjin 300134, P.R. China
E-mail: xfx22081@vip.163.com
E-mail: sun_peipei220@hotmail.com

*Contributed equally

Abbreviations: AMPK, adenosine monophosphate-activated protein kinase; ATP, adenosine triphosphate; BW, body weight; BUN, blood urea nitrogen; CCK-8, Cell Counting Kit-8; CKD, chronic kidney disease; CMC, carboxymethyl cellulose; Cr, creatinine; DM, diabetes mellitus; DN, diabetic nephropathy; ESRD, end-stage renal disease; FBG, fasting blood glucose; Gla, glargine; HG, high glucose; mALB, microalbumin; MFN, mitofusin; MMP, mitochondrial membrane potential; OPA1, optic atrophy protein 1; PGC-1α, peroxisome proliferator-activated receptor-γ co-activator-1α; TCM, Traditional Chinese Medicine; TEM, transmission electron microscopy

Key words: DN, mitochondrial dysfunction, apoptosis, Jinlida granules, AMPK, PGC-1α

Introduction

Due to improved living standards, life pattern changes and the aging of the society, the incidence of diabetes mellitus (DM) continues to escalate annually (1). On the basis of the International Diabetes Federation Global Diabetes Map 2021, there are currently 537 million patients with diabetes (range, 20-79 years old) worldwide, accounting for 10.5% of the total global population (2). It has been reported that 20-40% of individuals with diabetes develop diabetic nephropathy (DN), a microvascular complication of DM (3). Although previous studies indicated that renin-angiotensin system blockers could delay the onset of DN, they failed to halt the progression of the end-stage renal disease (ESRD). Therefore, emphasis should be placed on the early detection and interventions for DN. Additionally, elucidating the early mechanism of DN development for preventing and delaying disease progression is of great importance.

Glomerular podocyte loss is recognized as a critical element in the development of proteinuria, glomerulosclerosis and deterioration of renal function in DN (4). Mitochondria play a

crucial role in cellular energy production and several cellular processes, including antioxidant defense, calcium homeostasis and apoptosis (5). Most importantly, oxidative phosphorylation (OXPHOS) in mitochondria is associated with the synthesis of adenosine triphosphate (ATP), thus providing energy for different cellular functions (6,7). Mitochondria are organelles that are constantly undergoing dynamic changes. Therefore, maintaining the normal mitochondrial morphology to maximize ATP production is of great significance. Dynamic changes in fission, fusion and autophagy substantially depend on mitochondrial structure and morphology, which subsequently govern mitochondrial dynamics (8). A previous study demonstrated that OXPHOS was increased in mitochondrial fusion and decreased in mitochondrial fission (9). Additionally, enhanced fission and reduced fusion, causing podocyte mitochondrial breakage, were significantly associated with the development of DN (10). Therefore, maintaining dynamic mitochondrial homeostasis in podocytes could be an effective therapeutic strategy for DN (3).

Over the past few years, the application of Traditional Chinese Medicine (TCM) in the field of medical science has been gradually recognized by both domestic and foreign counterparts (11). Emerging evidence has supported the unique advantages of TCM in preventing DM progression (12,13). Therefore, it is meaningful to investigate the effective constituents of TCM for managing DM. A large randomized clinical trial (FOCUS) revealed that Jinlida granules (JLD) reduced the risk of diabetes in subjects with metabolic abnormalities (14). JLD is composed of 17 Chinese herbs, including *Ginseng*, *Polygonum multiflorum*, *Salvia miltiorrhiza*, *Sophora flavescens*, *Rehmannia glutinosa*, Epimedium, *Rhizoma coptidis*, *Atractylodes lancea preparata*, *Radix ophiopogonis*, *Polygonum multiflorum*, *Cornus officinalis*, *Polyporia cocos*, *Eupatorium fortunei*, *Rhizoma anemarrhenae*, *Pachyrhizua angulatus*, *Semen litchi* and *Cortex lycii radices,* with known therapeutic effects. JLD, an innovative TCM formulation, is developed based on empirical knowledge guided by the theory of 'collateral disease'. This compound can effectively strengthen the spleen and against phlegm and moisture overload (15) Previous studies revealed that JLD exerted a positive effect on improving insulin resistance and regulating disruptions in glucose and lipid metabolism (15,16). However, the particular mechanism underlying the effects of JLD on DN remains unclear. Therefore, the current study aimed to investigate the therapeutic effects of JLD on DN and its relative molecular mechanism, thus highlighting the possible key role of JLD in podocyte apoptosis via the adenosine monophosphate-activated protein kinase (AMPK)/peroxisome proliferator-activated receptor-γ co-activator-1α (PGC-1α) pathway to ameliorate mitochondrial dysfunction.

Materials and methods

Reagents. JLD was obtained from Shijiazhuang Yiling Pharmaceutical Co., Ltd. and was pulverized into ultrafine powder. Valsartan (Val) was purchased from Nova Beijing Pharmaceutical Co., Ltd., while insulin glargine (Gla) from Sanofi Beijing Pharmaceutical Co., Ltd. JLD and Val were individually dissolved in 0.5% sodium carboxymethyl cellulose (CMC) for intragastric administration. Gla was administered by subcutaneous injection.

Animals. In the present study, animal experiments were ethically approved by the Animal Ethical Committee of the Tianjin Medical University Chu Hsien-I Memorial Hospital (approval no. 2022084; Tianjin, China). SPF grade male db/m and db/db mice (age, 7 weeks-old; weight, 35-40 g) were purchased from Gempharmatech Co., Ltd. and maintained in the Laboratory Animal Center. Mice were maintained at a temperature of 23±3˚C, humidity of 45±15%, and a 12/12-h light/dark cycle with free access to food and water. Following acclimatization for two weeks, mice were then allocated into the following six groups: control (db/m), model (db/db), Val (db/db + 10 mg /kg/d Val), Gla (db/db + 3 U/kg/d Gla), JLD-L (db/db + 1.75 g/kg/d JLD) and JLD-H (db/db + 3.5 g/kg/d JLD) groups (n=10 mice/group). At the age of nine weeks, mice were daily treated with JLD, Val or an equal volume of CMC for eight weeks. After 12 h of fasting, blood from the tail tip of the mice was collected and fasting blood glucose (FBG) was measured using a glucometer. FBG and body weight (BW) levels were recorded weekly throughout the experimental period. At the end of administration, mice entered the metabolic system for metabolic data monitoring and urine were collected by metabolic cage. Blood and kidneys were collected following mice euthanasia by 30-70% vol/min CO_2 absorption. Following euthanasia, mice were examined for cardiac arrest, respiratory arrest, body rigidity and dilated pupils to confirm animal death. If the mice were not already dead, cervical dislocation followed.

Detection of renal function indicators. Urinary albumin content (cat. no. JL20493-96T) was measured using the corresponding ELISA kit. In addition, creatinine (Cr, cat. no. JL-T0928-96) and blood urea nitrogen (BUN, cat. no. JL-T1014-96) kits were provided by Jianglai Biotechnology (Jianglaibio) Co., Ltd.

Histopathological staining of kidney tissue sections. Following fixed with 4% formaldehyde for 24 h at 4˚C, the kidney tissues were cut into 4-μm thick slices and embedded in paraffin. Subsequently, the slices were stained with hematoxylin and eosin (H&E) and observed under a light microscope (Olympus Corporation).

Transmission electron microscopy (TEM). Fresh renal cortex tissues were collected and fixed with 2% glutaraldehyde at 4˚C overnight. The tissues were inserted into the pure EMBed 812 (cat. no. 90529-77-4; SPI), and then kept at 37˚C overnight. A total of 2% uranium acetate saturated alcohol solution (avoiding light) was used for staining for 8 min and 2.6% lead citrate (avoiding CO_2) was used for staining for 8 min at room temperature. Following tissue section staining, images of the foot process and mitochondria were captured under TEM (Hitachi High-Technologies Corporation).

Immunofluorescence staining. Renal tissue paraffin sections were placed in xylene and dewaxed in water using descending ethanol series, and then antigenically repaired. Subsequently, the tissue sections were sealed with 1% BSA (Beijing Solarbio Science & Technology Co., Ltd.). and incubated with a primary antibody at 4˚C overnight. The primary antibodies used were the following: Anti-NPHS2 (1:200; cat. no. ab229037; Abcam), anti-SYNPO (1:200; cat. no. 21064-1-AP; Proteintech Group, Inc.). Following tissue incubation with the corresponding

FITC-labeled secondary antibody (1:200; cat. no. S2003; Simubiotech) for 1 h at 37˚C, the sections were blocked using an anti-fluorescence quenching blocking solution containing DAPI (cat. no. S2110; Beijing Solarbio Science & Technology Co., Ltd.) for 10 min at 4˚C. Images of the stained tissues were captured under a laser scanning confocal microscope (Carl Zeiss AG) or standard microscope (Olympus Corporation). The images were analyzed using ImageJ 1.53v software (National Institutes of Health).

TUNEL assay. Apoptotic cells in renal tissue sections were assessed using a TUNEL reagent for 15 min at 37˚C (Beyotime Institute of Biotechnology). Cell nuclei were stained with DAPI (cat. no. S2110; Beijing Solarbio Science & Technology Co., Ltd.) for 10 min at 4 ˚C. The apoptotic cells indicated by red fluorescence were observed under a fluorescent microscope.

Cell culture. Conditional permanent MPC5 cells were provided by Professor Mingzhen Li (Tianjin Medical University Chu Hsien-I Memorial Hospital). Cells were cultured in RPMI-1640 medium supplemented with 11.1 mM glucose (Gibco; Thermo Fisher Scientific, Inc.), 100 U/ml penicillin, 1% streptomycin (100 μg/ml) and 10% fetal bovine serum (Gibco; Thermo Fisher Scientific, Inc.) at 37˚C in an incubator with 5% CO_2. After reaching 80% confluence, MPC5 cells were exposed to glucose (MilliporeSigma) or mannitol (MA), as control. MPC5 cells were then treated with 50 (JLD-L), 100 (JLD-M) and 200 μg/ml (JLD-H) JLD or Val (2 μmol/l; cat. no. HY-18204; MedChemExpress) or AICAR (1 mmol/l; cat. no. HY-13417; MedChemExpress) or Compound C (5 μmol/l; cat. no. HY-13418A; MedChemExpress) in a high glucose (HG; 25 mmol/l) environment. MPC5 cells were then allocated into the following groups: The normal glucose, MA, HG, HG + Val, HG + JLD-L, HG + JLD-M, HG + JLD-H, HG + AICAR, HG + AICAR + JLD, HG + Compound C and HG + Compound C + JLD groups.

Cell viability assay. A Cell Counting Kit-8 (CCK-8) assay (Invigentech, Inc.) was carried out to assess the viability of cells. Briefly, MPC5 cells were cultured for 24 h at 37˚C with 5% CO_2. When the cell density reached 80%, cells were treated with 50, 100, 200, 400 and 800 μg/ml JLD or 11.1, 16.7, 25, 33.3 and 50 mmol/l glucose solution for an additional 24 h. Each well was then supplemented with 10 μl CCK-8 reagent and MPC5 cells were cultured for 1 h at 37˚C in an incubator. Finally, the absorbance at a wavelength of 450 nm was measured by an enzyme marker (Bio-Tek Instruments, Inc.).

Reactive oxygen species (ROS) and MitoSOX assay. ROS content in cells was determined using fluorescent probe dihydroethidium (DHE; US Everbright Inc.) staining and cell fluorescence was observed under a fluorescent microscope (Olympus Corporation). In addition, superoxide levels in mitochondria of living cells were monitored by MitoSOX (ABclonal Biotech Co., Ltd.) assay. Red fluorescence was observed under a fluorescent microscope (Olympus Corporation).

Mitochondrial membrane potential (MMP). MMP was assessed using a corresponding kit (cat. no. M8650; Beijing Solarbio Science & Technology Co., Ltd.). Briefly, MPC5 cells were cultured in confocal dishes and following cell staining with JC-1 for 20 min at 37˚C, and living cells were observed under a confocal microscope.

Assessment of mitochondrial DNA (mtDNA) copy numbers. Total DNA was extracted from kidney tissues and MPC5 cells using a DNA extraction kit (cat. no. D1700; Beijing Solarbio Science & Technology Co., Ltd.). Using gene-specific PCR primers synthesized by Tsingke Biotechnology Co., Ltd., quantitative PCR was employed to determine mtDNA copy number. Enzyme activation at 93˚C (10 min), denaturation at 93˚C (15 sec), annealing at 55˚C (30 sec) and extension at 72˚C (30 sec) followed by 40 cycles. The primer sequences used were as follows: mtND1 forward, 5'-ACCATTTGCAGA CGCCATAA-3' and reverse, 5'-TGAAATTGTTTGGGCTAC GG-3'; and β-globin forward, 5'-GAAGCGATTCTAGGG AGCAG-3' and reverse, 5'-GGAGCAGCGATTCTGAGT AGA-3'. The relative mtDNA content was ascertained via normalizing mtDNA expression to that of β-globin.

MitoTracker assay. A MitoTracker assay (Cell Signaling Technology, Inc.) was used to locate mitochondria in living MPC5 cells. Mitochondrial morphology was observed under a confocal microscope.

Flow cytometry. According to the manufacturer's protocol, the Annexin V-FITC apoptosis detection kit (cat. no. BB-4101-50T; BestBio Biotechnologies Co., Ltd.) was employed to stain MPC5 cells ($1x10^5$ cells/hole). Subsequently, apoptotic cells were identified using flow cytometry (model, BD FACSVerse; BD biosciences) and the data were analyzed using FlowJo 10.8.1 software (FlowJo LLC).

Cell transfection. For PGC-1α silencing, MPC5 cells were transfected with specific small interfering RNAs (siRNAs) targeting PGC-1α (concentration, 20 μmol/l; sense, 5'-GCCAAACCA ACAACUUUAUTT-3' and antisense, 5'-AUAAAGUUGUUG GUUUGGCTT-3') or normal control siRNAs (concentration, 20 μmol/l; sense, 5'-UUCUCCGAACGUGUCACGUTT-3' and antisense, 5'-ACGUGACACGUUCGGAGAATT-3') using the Lipofectamine® 2000 transfection reagent. After cell transfection for 6 h at 37˚C, the medium was changed, and the next 24 h after which the cells were intervened. Both siRNA sequences were provided by Shanghai GenePharma Co., Ltd. Transfected MPC5 cells were then treated with 25 mmol/l HG or 200 μg/ml JLD for the subsequent experiments.

Western blot analysis. Proteins were extracted from kidney tissues or MPC5 cells using a RIPA cracking buffer (cat. no. R0020; Beijing Solarbio Science & Technology Co., Ltd.), supplemented with phosphatase inhibitor (Calyculin A) and phenylmethylsulfonyl fluoride. Protein concentration was measured by the BCA method. The same quantity of protein extracts (20 μg) was separated by 10% SDS-PAGE and the proteins were then transferred onto nitrocellulose membranes. Following sealing in Tris-buffered solution (pH, 7.2-7.4), containing 10% Tween-20 and 5% skim milk, for 1 h, the membranes were incubated with primary antibodies at 4˚C overnight. The following day, the membrane was incubated with the Goat Anti-Rabbit HRP-conjugated

secondary antibody (1:5,000; cat. no. BS13278; Bioworld Technology, Inc.) for 1 h. The immunoreactive protein bands were visualized using an enhanced chemiluminescence kit (Beijing Solarbio Science & Technology Co., Ltd.) and analyzed using ImageJ software. The antibodies used were the following: Anti-NPHS2 (1:1,000; cat. no. ab229037; Abcam), anti-phosphorylated (p)- dynamin-related peptide 1 ($DRP1^{S616}$; 1:1,000; cat. no. 3455S; Cell Signaling Technology, Inc.), anti-p-$DRP1^{S637}$(1:1,000; cat. no. ab193216; Abcam), anti-PGC-1α (1:1,000; cat. no. ab54481; Abcam), anti-p-AMPK (1:1,000; cat . no. ab13448; Abcam) and anti-AMPK (1:1,000; cat. no. ab32047; Abcam); anti-optic atrophy protein 1 (OPA1; 1:1,000; cat. no. 880471S; Cell Signaling Technology, Inc.), anti-DRP1 (1:1,000; cat. no. 8570S; Cell Signaling Technology, Inc.) and anti-mitofusin 2 (MFN2; 1:1,000; cat. no. 9482S; Cell Signaling Technology, Inc.)); anti-synaptopodin (SYNPO; 1:1,000; cat. no. 21064-1-AP; Proteintech Group, Inc.), anti-BAX (1:2,000; cat. no. 50599-2-IG; Proteintech Group, Inc.), anti-BCL2 (1:2,000; cat. no. 26593-1-AP; Proteintech Group, Inc.) and anti-β-actin (1:2,000; cat. no. 20536-1-AP; Proteintech Group, Inc.); and anti-cleaved caspase 3 (1:1,000; cat. no. A2156; ABclonal Biotech Co., Ltd.).

RNA-sequencing. RNA sequencing was performed on fresh kidney tissues derived from mice in the db/m, db/db and db/db + JLD-H groups. Total RNA was extracted from kidney tissues using TRIzol reagent. Sample quality verification was performed using Fragment Analyzer (model, 5300; Agilent Technologies, Inc.). The library was prepared using the Optimal Dual-mode mRNA Library Prep Kit (cat. no. LR00R96; BGI, Inc.). Fragment Analyzer measured library loading concentrations at least 5 ng/μl. mRNA was enriched by oligo (dT)-attached magnetic beads and reversed transcribed into cDNA. Following cDNA end repairment, an A nucleotide was added to the blunt fragments. The single-stranded cyclized DNA products were replicated to construct DNA nanoballs (DNBs). DNBs were then loaded into the patterned nanoarray and paired end of 150 base reads were performed on the T7 platform (BGI, Inc.). Data were analyzed, visualized and mined using the 'Dr. Tom' system (https://biosys.bgi.com). The differentially expressed genes were identified using the DESeq2 v1.4.5 package, with Q≤0.05. Kyoto Encyclopedia of Genes and Genomes (KEGG; https://www.kegg.jp/) and Gene Ontology (GO; http://www.geneontology.org/) enrichment analyses were performed on differentially expressed genes with a Q value of ≤0.05. RNA-sequencing and analysis of results were performed by BGI Genomics Co., Ltd.

Statistical analyses. Graphical representations were created using GraphPad Prism 9.0 software (Dotmatics). All results are expressed as the mean ± SEM. The differences among multiple groups were compared by one-way ANOVA followed by Tukey's post hoc test, while those between two groups by unpaired Student's t-tests. $P<0.05$ was considered to indicate a statistically significant difference.

Results

JLD restores the kidney function of db/db mice. The results demonstrated that FBG and BW levels were significantly increased in db/db mice compared with db/m mice. Mice in JLD groups showed decreased FBG levels and BW compared with those in db/db group, thus supporting the hypoglycemic and weight loss effects of JLD (Fig. 1A and B). Furthermore, the urinary microalbumin/Creatinine (mALB/Cr) rate, and mALB and BUN levels were dose-dependently reduced in the JLD groups compared with the db/db group (Fig. 1C-E). Additionally, the renal function indicators were significantly improved in Val group (Fig. 1C-E). In addition, FBG levels, but not renal function, were also significantly improved in the Gla group (Fig. S1A-C). At the same time, energy metabolism was enhanced in db/db mice after JLD intervention (Fig. 1F-H). Overall, these findings indicated that JLD could effectively restore kidney function in the db/db group, possibly independently of its hypoglycemic effect.

JLD improves glomerular morphology and podocyte injury in db/db mice. As illustrated in Fig. 2A, the renal pathology of db/db mice was characterized by tubule dilatation and glomerular atrophy. TEM showed that the glomerular basement membrane thickened and the foot process was fused in db/db mice (Fig. 2B). However, glomerular morphology was improved in the JLD groups. Podocyte injury is generally considered as a critical step in the development of DKD. Therefore, in the present study, to assess podocyte injury, the expression levels of the functional- and podocyte-specific indicators NPHS2 and SYNPO were detected. Immunofluorescence and western blot results revealed that both NPHS2 and SYNPO were downregulated in db/db mice and their expression levels were restored following mice treatment with JLD (Fig. 2C-F). The aforementioned results demonstrated that JLD could significantly improve glomerular morphology and podocyte injury.

JLD inhibits cell apoptosis in db/db mice. To explore the molecular mechanism underlying the effect of JLD on improving renal function and podocyte injury, RNA sequencing and KEGG enrichment analyses were performed in the kidney tissues of mice. In the aforementioned animal experiments, the results demonstrated that the general condition and kidney injury in mice in the JLD-H group (db/db + 3.5 g/kg/d JLD) were improved more significantly. Therefore, the kidney tissues isolated from JLD-H group were selected for RNA sequencing. The analysis revealed that a total of 539 factors were upregulated in db/db group and downregulated in JLD group. Similarly, 151 factors were downregulated in db/db group and upregulated in JLD group (Fig. 3A-C). Furthermore, KEGG and GO enrichment analysis revealed that the differentially expressed genes were mainly clustered in apoptotic pathways (Fig. 3D). In addition, western blot analysis was performed to detect the apoptosis-related proteins, namely BAX, BCL2 and cleaved caspase 3. Therefore, cell apoptosis was enhanced in db/db mice compared with db/m mice, while it was restored in JLD groups (Fig. 3F and G). Consistently, TUNEL staining assays revealed that the number of apoptotic cells was increased in db/db group and reduced in JLD groups (Fig. 3E). Overall, the aforementioned findings indicated that JLD could markedly inhibit cell apoptosis in db/db mice.

JLD inhibits DRP1-mediated mitochondrial fission and alleviates mitochondrial dysfunction in db/db mice. In previous studies, excessive mitochondrial fission and mitochondrial

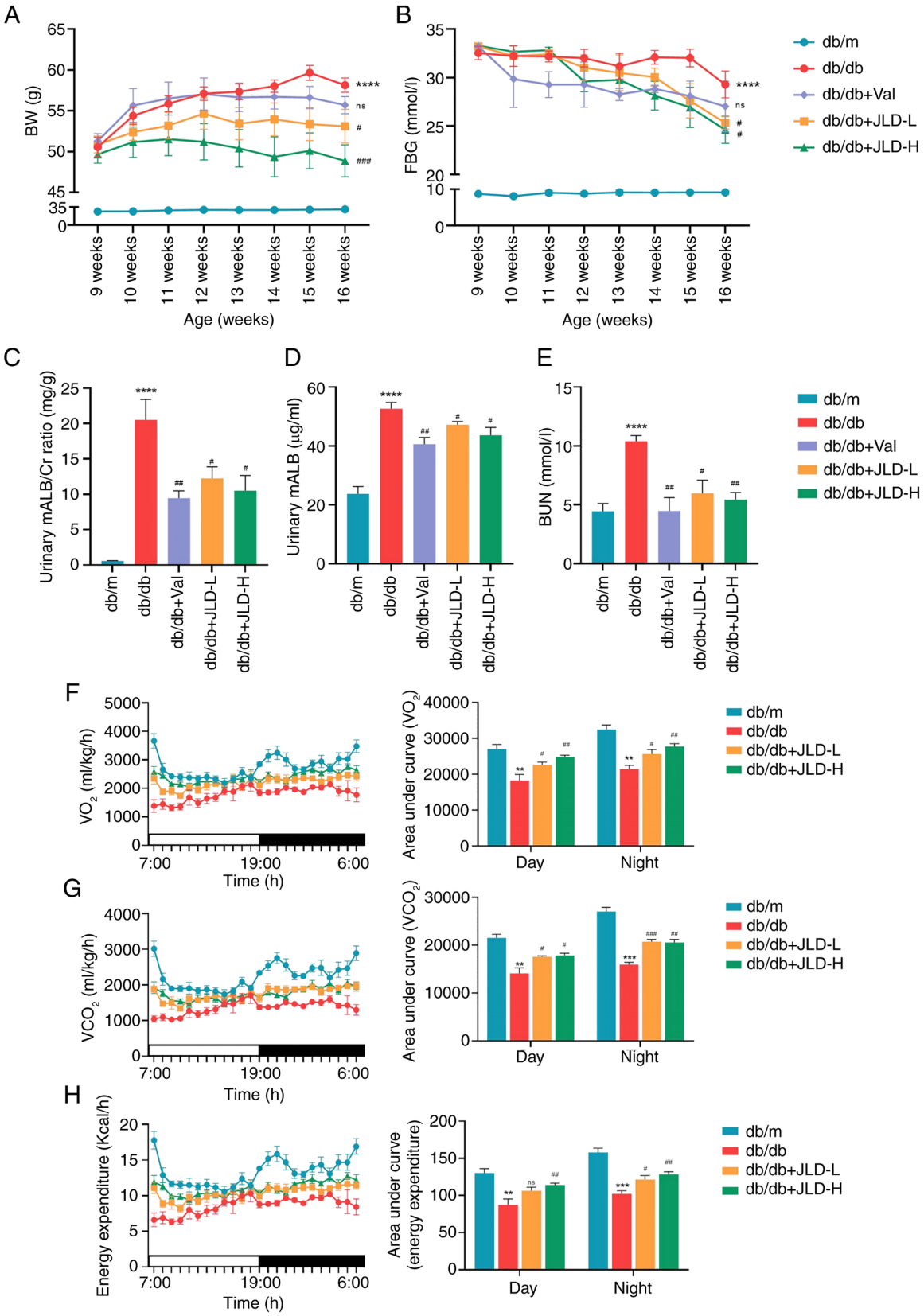

Figure 1. JLD restores the renal function of db/db mice. (A) BW. (B) FBG. (C) BUN. (D) mALB/Cr. (E) mALB. (F) O_2 consumption (VO_2). (G) CO_2 release quantity (VCO_2). (H) Energy expenditure. **P<0.01, ***P<0.001 and ****P<0.0001 vs. db/m group; $^{\#}$P<0.05, $^{\#\#}$P<0.01 and $^{\#\#\#}$P<0.001 vs. db/db group. JLD, Jinlida granules; BW, body weight; FBG, fasting blood glucose; BUN, blood urea nitrogen; mALB/Cr, microalbumin/creatinine; Val, Valsartan; ns, no significance.

dysfunction were observed in HG-induced MPC5 cells, thus resulting in enhanced ROS production and cell apoptosis (17,18). Consistently, in the present study, mitochondrial morphology and function were assessed. The results revealed that the morphology of mitochondria in the db/db group was characterized by abnormal structure, accompanied by

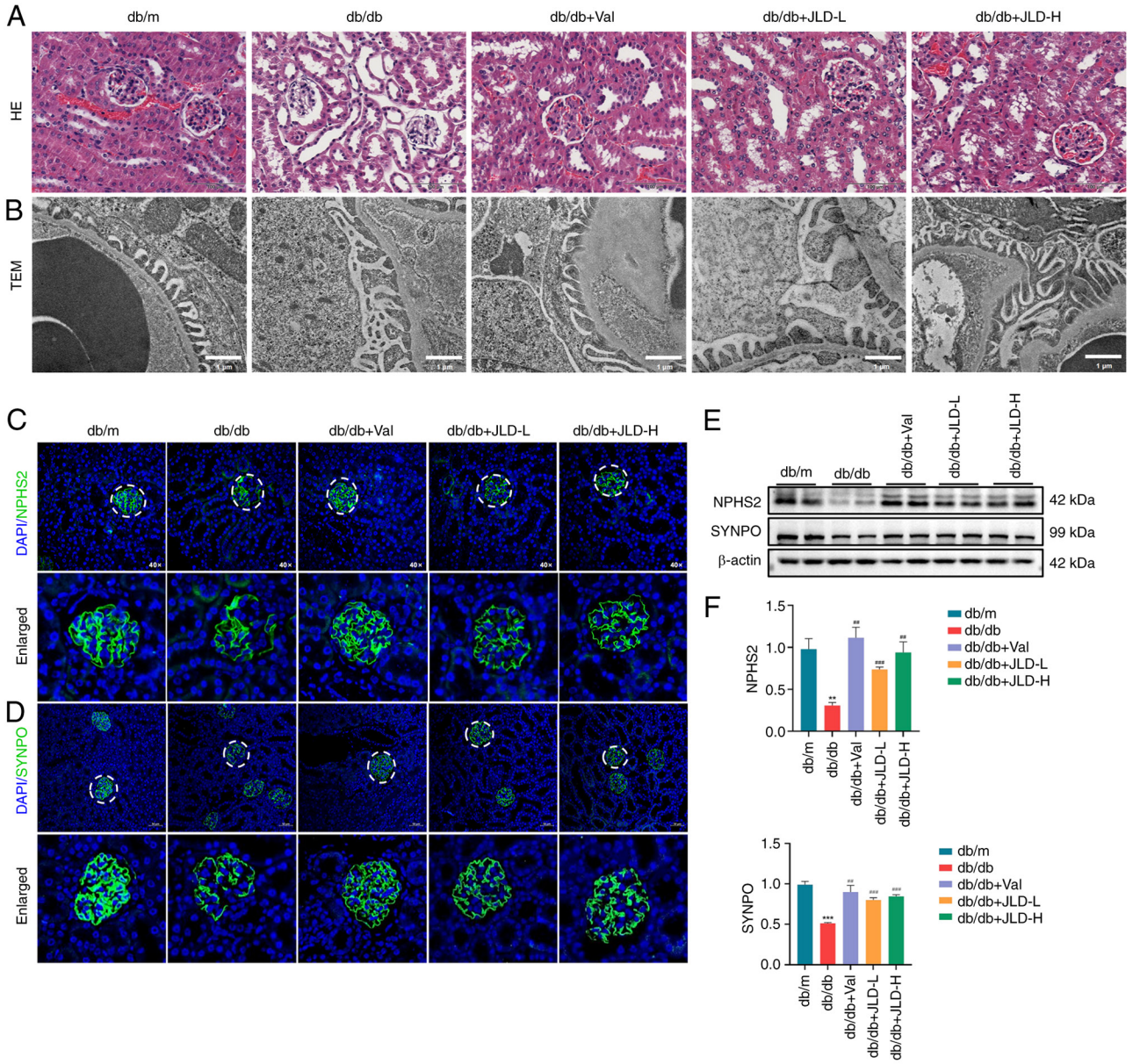

Figure 2. JLD improves glomerular morphology and podocyte injury of db/db mice. (A) H&E (scale bar, 100 μm). (B) TEM for foot process (scale bar, 1 μm). (C) Immunofluorescence of NPHS2 in kidneys (magnification, x40). (D) Immunofluorescence of SYNPO in kidneys (scale bar, 50 μm). (E and F) Relative protein expression of NPHS2 and SYNPO in mice. **P<0.01 and ***P<0.001 vs. db/m group; $^{\#\#}$P<0.01 and $^{\#\#\#}$P<0.001 vs. db/db group. JLD, Jinlida granules; TEM, transmission electron microscopy; SYNPO, synaptopodin; Val, Valsartan.

swelling, rupture and mitochondrial ridge reduction. However, the morphology of mitochondria was restored in mice in the JLD group (Fig. 4A). In db/db mice, p-DRP1^{S616} was upregulated and p-DRP1^{S637} was downregulated, while the protein expression levels of the mitochondrial fusion-related proteins, OPA1 and MFN2, were also reduced, thus suggesting that diabetic mice were characterized by enhanced mitochondrial division and decreased podocyte fusion (Fig. 4C and D). In addition, attenuated mitochondrial fission, decreased ROS levels and increased copy numbers of mtDNA were observed in mice in the JLD groups (Fig. 4B and E). These findings suggested that JLD could significantly inhibit mitochondrial division and alleviate mitochondrial dysfunction.

JLD alleviates HG-induced MPC5 cell apoptosis. To investigate the possible mechanisms by which JLD could improve cell apoptosis and mitochondrial dysfunction, hyperglycemia was simulated *in vitro* by treating MPC5 cells with HG. For CCK-8 assays, cells were co-treated with increasing concentrations of JLD (50, 100 and 200 μg/ml) and 25 mmol/l HG (Fig. 5A and B). In HG-treated MPC5 cells, apoptosis was increased, as evidenced by cleaved caspase 3 and BAX upregulation and BCL2 downregulation (Fig. 5C and D). Flow cytometry revealed that cell apoptosis was enhanced in podocytes induced by HG. However, this effect was reversed by JLD (Fig. 5E and F). These results verified that JLD could inhibit HG-induced podocyte apoptosis.

JLD alleviates mitochondrial fission and mitochondrial dysfunction in MPC5 cells. Consistent with the *in vivo* results, MitoTracker staining revealed mitochondrial fragmentation in HG-induced MPC5 cells (Fig. 6B). MMP upregulation and

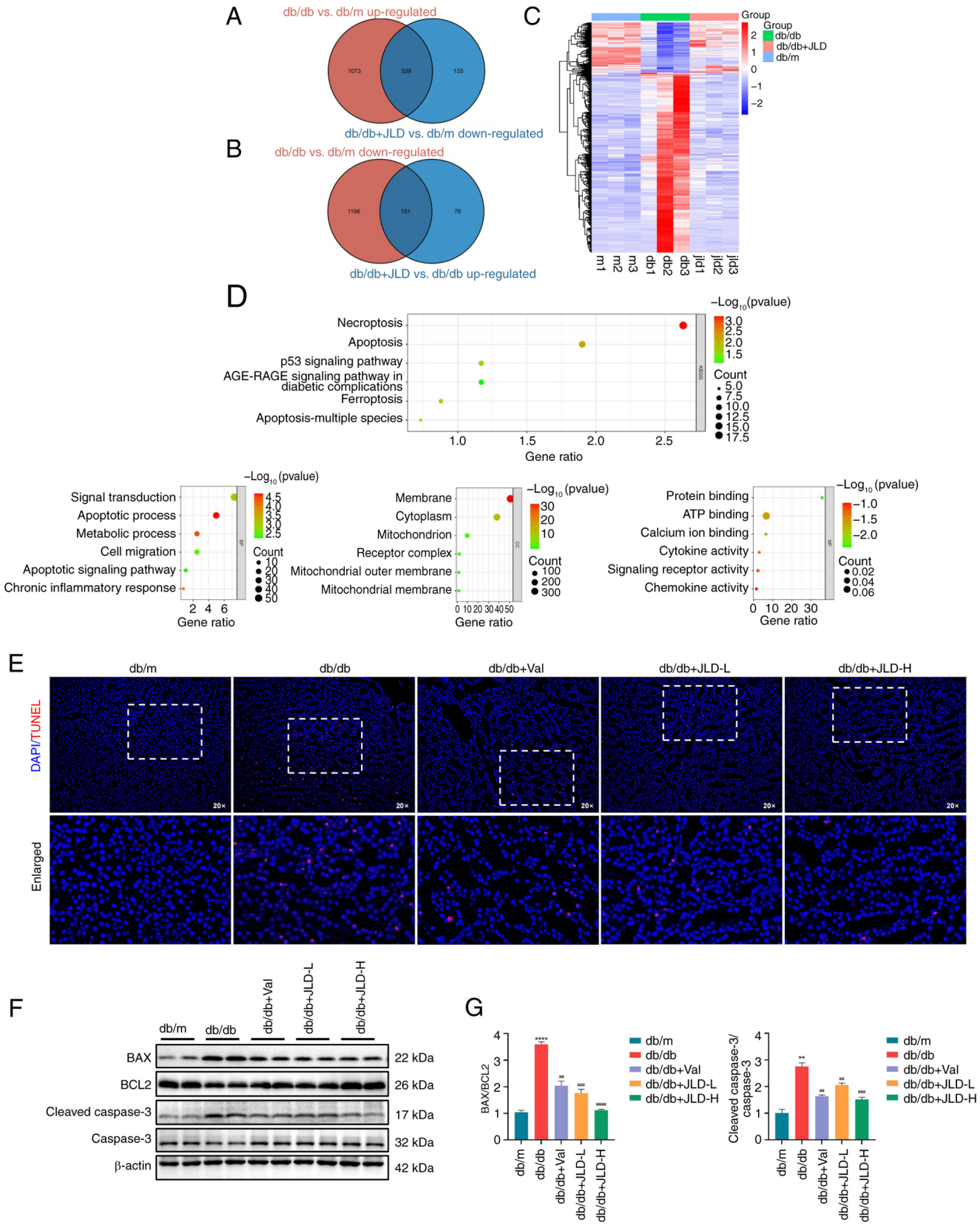

Figure 3. JLD inhibits apoptosis in db/db mice. (A) Venn diagram of genes in db/db upregulated and db/db + JLD downregulated. (B) Venn diagram of genes in db/db downregulated and db/db + JLD upregulated. (C) Clustering heat map between groups. (D) Kyoto Encyclopedia of Genes and Genomes and Gene Ontology enrichment analysis of different genes. (E) TUNEL staining (magnification, x20). (F and G) Relative protein expression of BAX, BCL2 and cleaved caspase 3 in mice. **P<0.01 and ****P<0.0001 vs. db/m group; $^{\#\#}$P<0.01, $^{\#\#\#}$P<0.001 and $^{\#\#\#\#}$P<0.0001 vs. db/db group. JLD, Jinlida granules; Val, Valsartan.

elevated mitochondrial ROS production are closely associated with mitochondrial dysfunction. Therefore, the results demonstrated that MMP was downregulated in HG-induced MPC5 cells, while JC-1 staining revealed mitochondrial

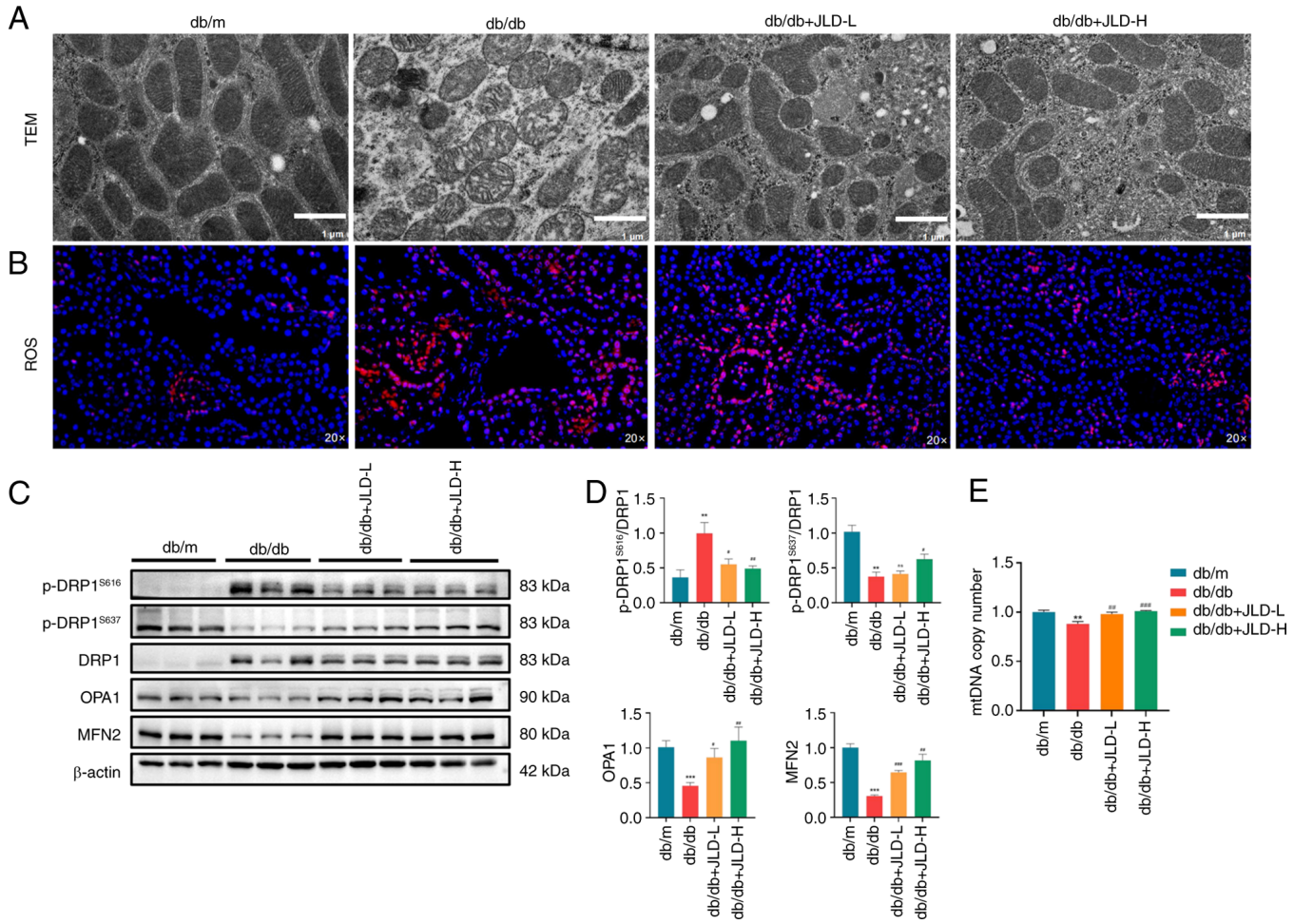

Figure 4. JLD inhibits DRP1-mediated mitochondrial fission and alleviates mitochondrial dysfunction of db/db mice. (A) TEM for mitochondria (scale bar, 1 μm). (B) ROS staining (magnification, x20). (C and D) Relative protein expression of p-DRP1^{S616}, p-DRP1^{S637}, DRP1, OPA1 and MFN2 in mice. (E) mtDNA copy number in each group. **P<0.01 and ***P<0.001 vs. db/m group; $^{\#}$P<0.05, $^{\#\#}$P<0.01 and $^{\#\#\#}$P<0.001 vs. db/db group. JLD, Jinlida granules; DRP1, dynamin-related peptide 1; TEM, transmission electron microscopy; ROS, reactive oxygen species; p-, phosphorylated; OPA1, optic atrophy protein 1; MFN, mitofusin; mtDNA, mitochondrial DNA.

depolarization. The aforementioned effects were reversed by JLD administration (Fig. 6A). In addition, MitoSOX staining demonstrated that ROS production was increased in HG-induced podocytes, and it was significantly reduced by JLD (Fig. 6C). Furthermore, the western blot analysis results indicated that HG-induced MPC5 cells displayed excessive mitochondrial division and decreased mitochondrial fusion, which were reversed following treatment with JLD (Fig. 6D and E). Finally, the RT-qPCR results identified that JLD could restore the reduced copy number of mtDNA in HG-induced podocytes (Fig. 6F). Overall, these findings verified that JLD could significantly inhibit mitochondrial division and improve mitochondrial dysfunction.

JLD alleviates mitochondrial division and apoptosis via activating the AMPK/PGC-1α pathway. AMPK and PGC-1α serve critical roles in the maintenance of mitochondrial homeostasis. Therefore, dysfunction of this pathway has been related to the pathogenesis of several metabolic diseases, such as diabetes (19,20). To explore whether the AMPK/PGC-1α pathway participates in the JLD-mediated podocyte apoptosis and mitochondrial dysfunction improvement, the *in vivo* and *in vitro* protein expression levels of AMPK/PGC-1α were detected. The analysis showed that AMPK phosphorylation and PGC-1α expression were reduced in the db/db group, while they were significantly enhanced in JLD groups (Fig. 7A and B). Consistent with the *in vivo* results, the phosphorylation levels of AMPK/PGC-1α expression were decreased in HG-induced podocytes, which were reversed after JLD intervention (Fig. 7C and D). Therefore, it was hypothesized that JLD could ameliorate podocyte apoptosis and mitochondrial dysfunction via the AMPK/PGC-1α pathway. The aforementioned finding was verified following MPC5 cell treatment with AICAR, an AMPK activator, or its inhibitor, compound C. Therefore, p-AMPK and PGC-1α were downregulated in HG- and compound C-intervened MPC5 cells, thus promoting excessive mitochondrial division and apoptosis. However, HG-induced MPC5 cell treatment with JLD and AICAR displayed the opposite effect (Fig. 7E, G-I). To further support that PGC-1α could be considered as a critical factor in JLD action to ameliorate mitochondrial dysfunction and apoptosis in podocytes, MPC5 cells were transfected with siRNA clones targeting PGC-1α (Fig. S2). As expected, PGC-1α knockdown abrogated the effects of JLD on ameliorating excessive mitochondrial division and apoptosis

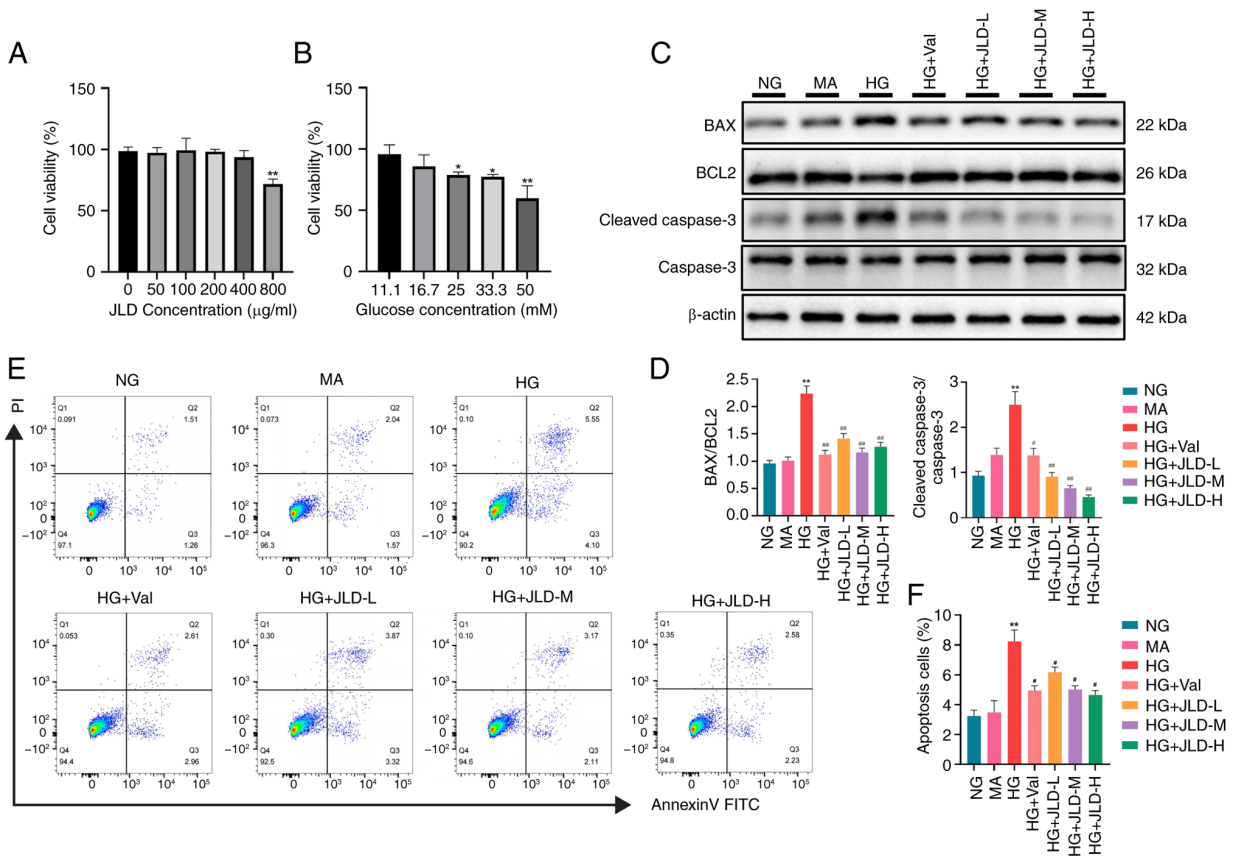

Figure 5. JLD alleviates apoptosis induced by HG in MPC5 cells. (A) Cell viability at different JLD concentrations. (B) Cell viability at different glucose concentrations. (C and D) Relative protein expression of BAX, BCL2 and Cleaved Caspase 3 in MPC5 cells. (E and F) The Annexin V/PI staining of apoptotic rate. **P<0.01 vs. NG group; $^{\#}$P<0.05 and $^{\#\#}$P<0.01 vs. HG group. JLD, Jinlida granules; HG, high glucose; NG, normal glucose; MA, mannitol; Val, Valsartan.

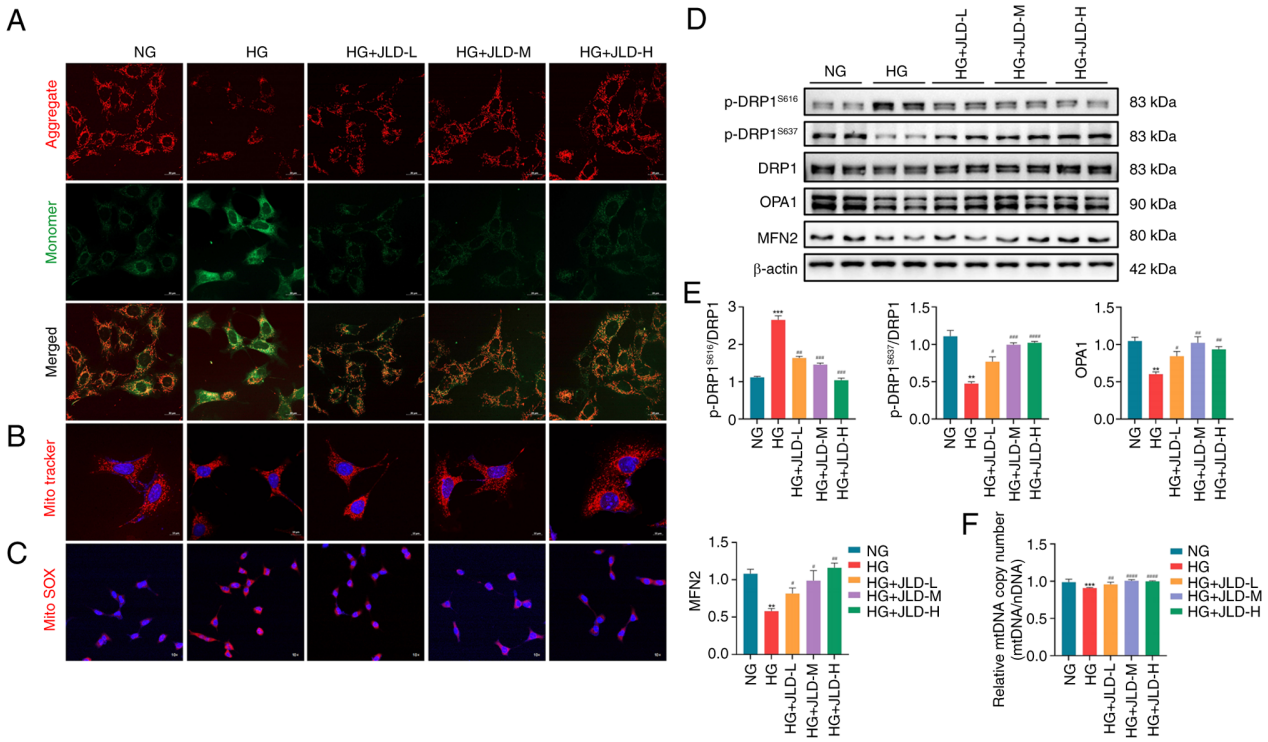

Figure 6. JLD alleviates mitochondrial fission and mitochondrial dysfunction induced by HG in MPC5 cells. (A) JC-1 staining (scale bar, 20 μm). (B) Mito Tracker staining (scale bar, 20 μm). (C) MitoSOX staining (magnification, x10). (D and E) Relative protein expression of p-DRP1^{S616}, p-DRP1^{S637}, DRP1, OPA1 and MFN2 in MPC5. (F) mtDNA copy number in each group. **P<0.01 and ***P<0.001 vs. NG group; $^{\#}$P<0.05, $^{\#\#}$P<0.01, $^{\#\#\#}$P<0.001 and $^{\#\#\#\#}$P<0.0001 vs. HG group. JLD, Jinlida granules; HG, high glucose; p-, phosphorylated; DRP1, dynamin-related peptide 1; OPA1, optic atrophy protein 1; MFN, mitofusin; mtDNA, mitochondrial DNA; NG, normal glucose.

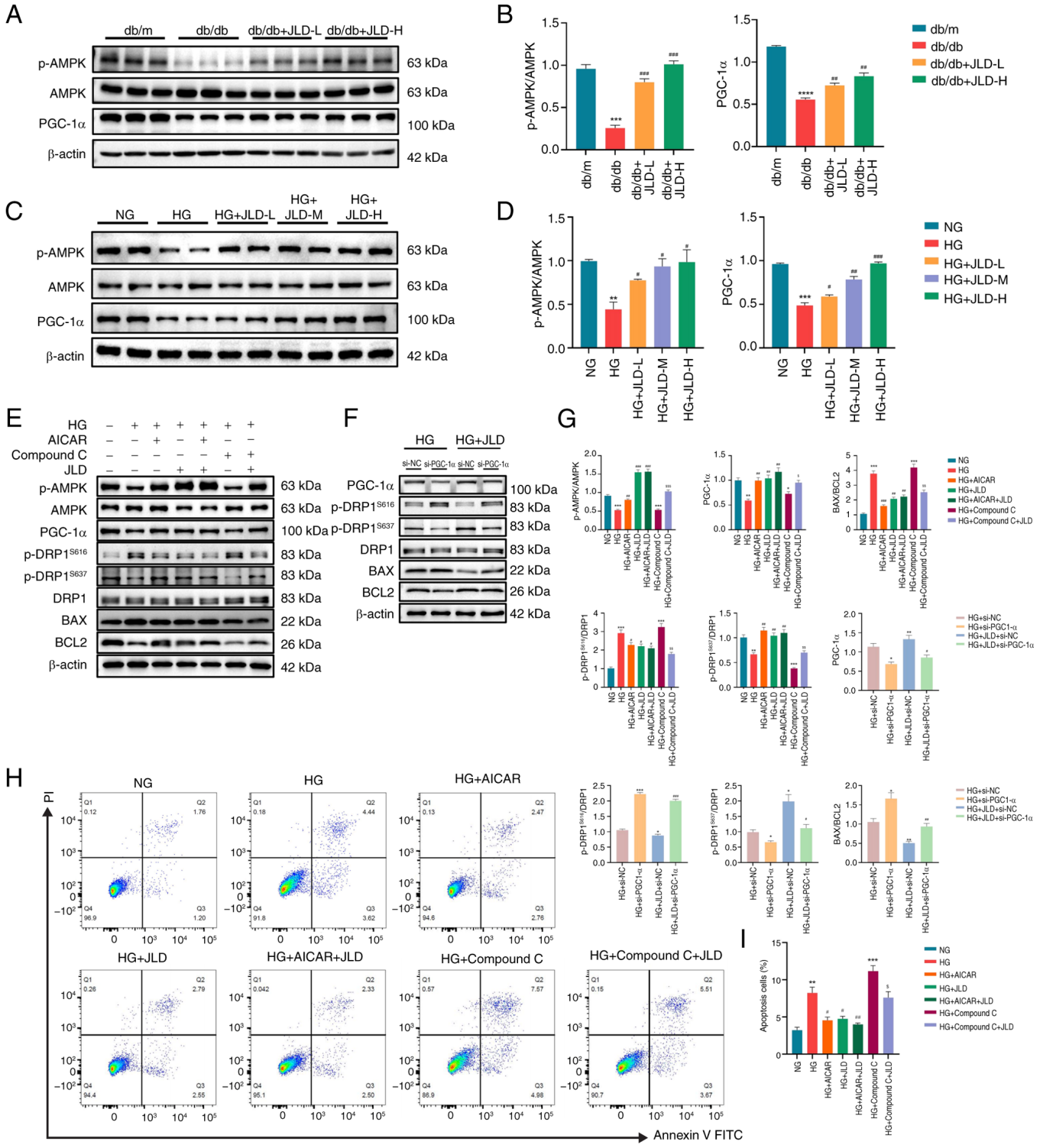

Figure 7. JLD alleviates mitochondrial division and apoptosis by activating the AMPK/PGC-1α pathway. (A and B) Relative protein expression of p-AMPK and PGC-1α in mice. (C and D) Relative protein expression of p-AMPK and PGC-1α in MPC5 cells. (E-G, H, I) MPC5 cells were treated with or without JLD (200 μg/ml), with or without AICAR (1 mmol/l), and with or without Compound C (5 μmol/l). Relative protein expression of p-AMPK, PGC-1α, p-DRP1^{S616}, p-DRP1^{S637}, DRP1, BAX and BCL2 in MPC5 cells. The Annexin V/PI staining of apoptotic rate in each group. (F and G) MPC5 were transfected with si-NC or PGC-1α siRNA (si-PGC-1α) and then treated with or without JLD (200 μg/ml). Relative protein expression of PGC-1α, p-DRP1^{S616}, p-DRP1^{S637}, DRP1, BAX and BCL2 in MPC5 cells. $^{\$}$P<0.05, $^{\$\$}$P<0.01 and $^{\$\$\$}$P<0.001 vs. HG + Compound C group; *P<0.05, **P<0.01 and ***P<0.001 vs. HG + si-NC group; $^{\#}$P<0.05, $^{\#\#}$P<0.01 and $^{\#\#\#}$P<0.001 vs. HG + JLD + si-NC group. JLD, Jinlida granules; AMPK, adenosine monophosphate-activated protein kinase; PGC-1α, peroxisome proliferator-activated receptor-γ co-activator-1α; p-, phosphorylated; DRP1, dynamin-related peptide 1; siRNA, small interfering RNA; NC, negative control; HG, high glucose; NG, normal glucose.

in podocytes (Fig. 7F and G). To summarize, the aforementioned results confirmed that PGC-1α could be considered as a key effector of JLD in ameliorating apoptosis and mitochondrial dysfunction in podocytes through the AMPK pathway.

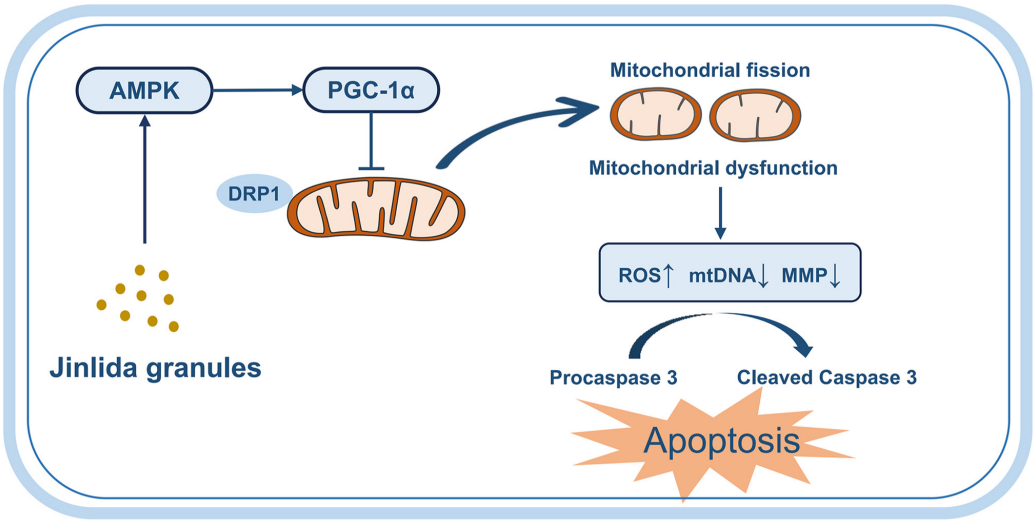

Figure 8. Schematic illustration of the mechanism. PGC-1α, peroxisome proliferator-activated receptor-γ co-activator-1α; AMPK, adenosine monophosphate-activated protein kinase; ROS, reactive oxygen species; mtDNA, mitochondrial DNA; DRP1, dynamin-related peptide 1; MMP, mitochondrial membrane potential.

Discussion

Diffuse thickening of the glomerular basement membrane, dilatation of the tethered membranes and nodular sclerosis (Kimmelstiel-Wilson nodules) are hallmark histopathological features of DN, which accounts for ~50% of all cases of chronic kidney disease (CKD) (21,22). As a complication of DM, DN is significantly involved in ESRD. Despite the prevalence and severity of DN, the benefits of the current therapeutic interventions remain limited. The results of the present study showed that JLD could protect against DN and effectively restore renal function.

Lower glomerular filtration rate and persistent proteinuria are hallmarks of DN. In patients with DN, podocyte damage and peduncle fusion are the primary manifestations of proteinuria. Since podocytes are terminally differentiated cells, DN progresses irreversibly if >20% of them are lost (23). In the present study, RNA sequencing and *in vitro*/*in vivo* experiments showed that the protective effect of JLD on podocytes was mediated via diminishing podocyte injury and apoptosis. It has been reported that podocytes can maintain their complex structure via regulating the cytoskeleton and extracellular matrix, which require substantial mitochondrial energy supply (24). Mitochondria are the major source of cellular energy and their dysfunction is notably associated with podocyte injury in patients with DN. Their dysfunction is affected by mitochondrial biogenesis, fusion and fission (25). Mitochondrial fission and fusion are mutually complementary processes that reinforce each other to maintain mitochondrial function and morphology. The aforementioned two processes can be achieved by cleavage and junction of the inner and outer mitochondrial membrane. Fusion is fundamental for homogenization of mitochondrial dynamics across the cellular mitochondrial network and enhances the efficiency of mitochondrial reactions (26). By contrast, mitochondrial fission is generally related to metabolic stress, thus severely contributing to mitochondrial degradation and apoptosis (25). Mitochondrial fusion is facilitated by MFN1 and MFN2, located in the outer mitochondrial membrane, and OPA1, located in the inner mitochondrial membrane (27). Fission is dominantly regulated by DRP1 and it can be accelerated by either increased DRP1 activity or DRP1 translocation to the outer mitochondrial membrane. Post-translational changes could affect DRP1 activity and translocation (28). For example, phosphorylating DRP1 at Ser-616 could promote fission, while DRP1 phosphorylation at Ser-637 could typically suppress this process (29,30). Herein, podocyte treatment with JLD reduced mitochondrial fission and improved mitochondrial dysfunction.

The regulation of cell growth, proliferation, differentiation, metabolism and survival is largely dependent on AMPK, which promotes the physiological development of various organs in the human body. The progression of DN and CKD can be facilitated by AMPK dysregulation (31,32). AMPK activity was reduced in HG-induced podocytes, thus altering cleft septa and cytoskeletal dysfunction. By contrast, regulating AMPK activity could affect actin dynamics and improve the architecture of foot process (33). In addition to AMPK inactivation, HG stimulation could also reactivate mammalian target of rapamycin pathway and induce apoptosis in podocytes (34). A previous study from our laboratory showed that JLD activated AMPK and enhanced autophagy in NIT-1 pancreatic β cells (15). Consistently, in the present study, JLD acted as an activator of AMPK, which not only ameliorated the structure of foot process but also attenuated podocyte apoptosis.

PGC-1α is a transcriptional coactivator that acts via responding to mitochondrial biogenesis and energy consumption (35,36). Apart from that, PGC-1α regulates mitochondrial dysfunction and mitochondrial quality control mechanisms (37). A previous research revealed a strong association between type 2 DM and genetic variations in PGC-1α (38). Furthermore, PGC-1α expression was markedly reduced in DN and CKD (39,40). Other studies verified that PGC-1α expression was primarily regulated by AMPK in diverse nephrotic diseases, including DN (41,42). The results revealed that JLD could possibly exert its pharmacological effect via activating AMPK to upregulate PGC-1α, which in

turn could ameliorate mitochondrial dysfunction. However, further investigation is needed to explore the mechanism by which JLD activates the phosphorylation of AMPK.

Another study suggested that that quercetin, luteolin and baicalin were the main active components of JLD, which acted against DM (43). Among them, quercetin is considered to have a protective role in podocyte apoptosis in DN (44). Several related bioactive compounds of JLD, such as puerarin and ginsenosides, have been considered to exhibit therapeutic effects against DN (45,46). To develop novel therapeutic strategies for DN, it is essential to find out the potential bioactive components of JLD and clarify how they affect mitochondrial homeostasis. The present study supported that JLD, a complex comprising multiple active ingredients, displayed therapeutic benefits in DN. JLD ameliorated podocyte apoptosis and mitochondrial dysfunction via the AMPK/PGC-1α pathway (Fig. 8).

As summarized, the current study described in detail the protective effects of JLD on podocytes from the perspective of mitochondrial function. The results indicated that JLD could be a potential activator of AMPK, which in turn mediated downstream PGC-1α factor to suppress podocyte apoptosis and mitochondrial fission. The aforementioned findings supported that JLD could serve as an effective therapeutic measure against DN and offer a novel insight into the molecular mechanisms of JLD in the treatment of this disease.

Acknowledgements

Not applicable.

Funding

The present study was supported by the project of Tianjin Health Committee Traditional Chinese Medicine and Integrated Traditional Chinese and Western Medicine Project (grant no. 2023152) and the Tianjin Key Medical Discipline (Specialty) Construction Project (grant no. TJYXZDXK-032A).

Availability of data and materials

The data generated in the present study may be found in the Genome Sequence Archive under accession number CRA019949 or at the following URL: https://ngdc.cncb.ac.cn/gsa/search?searchTerm=CRA019949.

Authors' contributions

SS conceptualized the study, wrote the original draft and conducted project administration. SY and YC developed methodology and performed formal analysis. TF performed software and formal analysis. JQ conducted investigation and data curation. LT developed methodology and conducted investigation. MZ validated data and conducted investigation. SW performed data validation and formal analysis. BS wrote, reviewed and edited the manuscript and conducted project administration. LC wrote, reviewed and edited the manuscript, conducted project administration and provided resources. SS, BS and LC confirm the authenticity of all the raw data. All authors read and approved the final version of the manuscript.

Ethics approval and consent to participate

Experimental procedures conducted in the present study were approved by the Animal Ethical Committee of Tianjin Medical University Chu HsienI Memorial Hospital (approval no. 2022084; Tianjin, China).

Patient consent for publication

Not applicable

Competing interests

The authors declare that they have no competing interests.

References

1. Tuttle KR, Agarwal R, Alpers CE, Bakris GL, Brosius FC, Kolkhof P and Uribarri J: Molecular mechanisms and therapeutic targets for diabetic kidney disease. Kidney Int 102: 248-260, 2022.
2. Magliano DJ and Boyko EJ; IDF Diabetes Atlas 10th edition Scientific Committee: Idf Diabetes Atlas. International Diabetes Federation © International Diabetes Federation, Brussels, 2021.
3. Cleveland KH and Schnellmann RG: Pharmacological targeting of mitochondria in diabetic kidney disease. Pharmacol Rev 75: 250-262, 2023.
4. Petrazzuolo A, Sabiu G, Assi E, Maestroni A, Pastore I, Lunati ME, Montefusco L, Loretelli C, Rossi G, Nasr MB, *et al*: Broadening horizons in mechanisms, management, and treatment of diabetic kidney disease. Pharmacol Res 190: 106710, 2023.
5. Dimmer KS and Scorrano L: (De)constructing mitochondria: What for? Physiology (Bethesda) 21: 233-241, 2006.
6. Bhargava P and Schnellmann RG: Mitochondrial energetics in the kidney. Nat Rev Nephrol 13: 629-646, 2017.
7. Flemming N, Pernoud L, Forbes J and Gallo L: Mitochondrial dysfunction in individuals with diabetic kidney disease: A systematic review. Cells 11: 2481, 2022.
8. Meyer JN, Leuthner TC and Luz AL: Mitochondrial fusion, fission, and mitochondrial toxicity. Toxicology 391: 42-53, 2017.
9. Mishra P, Carelli V, Manfredi G and Chan DC: Proteolytic cleavage of Opa1 stimulates mitochondrial inner membrane fusion and couples fusion to oxidative phosphorylation. Cell Metab 19: 630-641, 2014.
10. Forbes JM and Thorburn DR: Mitochondrial dysfunction in diabetic kidney disease. Nat Rev Nephrol 14: 291-312, 2018.
11. Wang X, Jiang L, Liu XQ, Huang YB, Wang AL, Zeng HX, Gao L, Zhu QJ, Xia LL and Wu YG: Paeoniflorin binds to VEGFR2 to restore autophagy and inhibit apoptosis for podocyte protection in diabetic kidney disease through PI3K-AKT signaling pathway. Phytomedicine 106: 154400, 2022.
12. Gong M, Guo Y, Dong H, Wu F, He Q, Gong J and Lu F: Modified Hu-lu-ba-wan protects diabetic glomerular podocytes via promoting PKM2-mediated mitochondrial dynamic homeostasis. Phytomedicine 123: 155247, 2024.
13. Shen Z, Cui T, Liu Y, Wu S, Han C and Li J: Astragalus membranaceus and Salvia miltiorrhiza ameliorate diabetic kidney disease via the 'gut-kidney axis'. Phytomedicine 121: 155129, 2023.
14. Ji H, Zhao X, Chen X, Fang H, Gao H, Wei G, Zhang M, Kuang H, Yang B, Cai X, *et al*: Jinlida for diabetes prevention in impaired glucose tolerance and multiple metabolic abnormalities: The FOCUS randomized clinical trial. JAMA Intern Med 184: 727-735, 2024.
15. Wang D, Tian M, Qi Y, Chen G, Xu L, Zou X, Wang K, Dong H and Lu F: Jinlida granule inhibits palmitic acid induced-intracellular lipid accumulation and enhances autophagy in NIT-1 pancreatic β cells through AMPK activation. J Ethnopharmacol 161: 99-107, 2015.
16. Zhang H, Hao Y, Wei C, Yao B, Liu S, Zhou H, Huang D, Zhang C and Wu Y: Chinese medicine Jinlida granules improve high-fat-diet induced metabolic disorders via activation of brown adipose tissue in mice. Biomed Pharmacother 114: 108781, 2019.

17. Susztak K, Raff AC, Schiffer M and Böttinger EP: Glucose-induced reactive oxygen species cause apoptosis of podocytes and podocyte depletion at the onset of diabetic nephropathy. Diabetes 55: 225-233, 2006.
18. Qin X, Zhao Y, Gong J, Huang W, Su H, Yuan F, Fang K, Wang D, Li J, Zou X, *et al*: Berberine protects glomerular podocytes via inhibiting Drp1-mediated mitochondrial fission and dysfunction. Theranostics 9: 1698-1713, 2019.
19. Steinberg GR and Hardie DG: New insights into activation and function of the AMPK. Nat Rev Mol Cell Biol 24: 255-272, 2023.
20. Handschin C and Spiegelman BM: Peroxisome proliferator-activated receptor gamma coactivator 1 coactivators, energy homeostasis, and metabolism. Endocr Rev 27: 728-735, 2006.
21. Mohandes S, Doke T, Hu H, Mukhi D, Dhillon P and Susztak K: Molecular pathways that drive diabetic kidney disease. J Clin Invest 133: e165654, 2023.
22. Tervaert TW, Mooyaart AL, Amann K, Cohen AH, Cook HT, Drachenberg CB, Ferrario F, Fogo AB, Haas M, de Heer E, *et al*: Pathologic classification of diabetic nephropathy. J Am Soc Nephrol 21: 556-563, 2010.
23. Mukhi D and Susztak K: The transcriptomic signature of the aging podocyte. Kidney Int 98: 1079-1081, 2020.
24. Liu S, Yuan Y, Xue Y, Xing C and Zhang B: Podocyte injury in diabetic kidney disease: A focus on mitochondrial dysfunction. Front Cell Dev Biol 10: 832887, 2022.
25. Audzeyenka I, Bierżyńska A and Lay AC: Podocyte bioenergetics in the development of diabetic nephropathy: The role of mitochondria. Endocrinology 163: bqab234, 2022.
26. Haroon S and Vermulst M: Linking mitochondrial dynamics to mitochondrial protein quality control. Curr Opin Genet Dev 38: 68-74, 2016.
27. Song M and Dorn GW II: Mitoconfusion: Noncanonical functioning of dynamism factors in static mitochondria of the heart. Cell Metab 21: 195-205, 2015.
28. Sabouny R and Shutt TE: Reciprocal regulation of mitochondrial fission and fusion. Trends Biochem Sci 45: 564-577, 2020.
29. Hu Q, Zhang H, Cortés NG, Wu D, Wang P, Zhang J, Mattison JA, Smith E, Bettcher LF, Wang M, *et al*: Increased Drp1 acetylation by lipid overload induces cardiomyocyte death and heart dysfunction. Circ Res 126: 456-470, 2020.
30. Tilokani L, Nagashima S, Paupe V and Prudent J: Mitochondrial dynamics: Overview of molecular mechanisms. Essays Biochem 62: 341-360, 2018.
31. Huynh C, Ryu J, Lee J, Inoki A and Inoki K: Nutrient-sensing mTORC1 and AMPK pathways in chronic kidney diseases. Nat Rev Nephrol 19: 102-122, 2023.
32. Juszczak F, Caron N, Mathew AV and Declèves AE: Critical role for AMPK in metabolic disease-induced chronic kidney disease. Int J Mol Sci 21: 7994, 2020.
33. Rogacka D, Audzeyenka I and Piwkowska A: Regulation of podocytes function by AMP-activated protein kinase. Arch Biochem Biophys 692: 108541, 2020.
34. Eid AA, Ford BM, Bhandary B, de Cassia Cavaglieri R, Block K, Barnes JL, Gorin Y, Choudhury GG and Abboud HE: Mammalian target of rapamycin regulates Nox4-mediated podocyte depletion in diabetic renal injury. Diabetes 62: 2935-2947, 2013.
35. Li SY and Susztak K: The role of peroxisome proliferator-activated receptor γ coactivator 1α (PGC-1α) in kidney disease. Semin Nephrol 38: 121-126, 2018.
36. Fontecha-Barriuso M, Lopez-Diaz AM, Guerrero-Mauvecin J, Miguel V, Ramos AM, Sanchez-Niño MD, Ruiz-Ortega M, Ortiz A and Sanz AB: Tubular mitochondrial dysfunction, oxidative stress, and progression of chronic kidney disease. Antioxidants (Basel) 11: 1356, 2022.
37. Halling JF and Pilegaard H: PGC-1α-mediated regulation of mitochondrial function and physiological implications. Appl Physiol Nutr Metab 45: 927-936, 2020.
38. Wu H, Deng X, Shi Y, Su Y, Wei J and Duan H: PGC-1α, glucose metabolism and type 2 diabetes mellitus. J Endocrinol 229: R99-R115, 2016.
39. Ji JL, Li JY, Liang JX, Zhou Y, Liu CC, Zhang Y, Zhang AQ, Liu H, Ma RX and Li ZL: Tubular TMEM16A promotes tubulointerstitial fibrosis by suppressing PGC-1α-mediated mitochondrial homeostasis in diabetic kidney disease. Cell Mol Life Sci 80: 347, 2023.
40. Fontecha-Barriuso M, Martin-Sanchez D, Martinez-Moreno JM, Monsalve M, Ramos AM, Sanchez-Niño MD, Ruiz-Ortega M, Ortiz A and Sanz AB: The role of PGC-1α and mitochondrial biogenesis in kidney diseases. Biomolecules 10: 347, 2020.
41. Hou S, Zhang T, Li Y, Guo F and Jin X: Glycyrrhizic acid prevents diabetic nephropathy by activating AMPK/SIRT1/PGC-1α signaling in db/db Mice. J Diabetes Res 2017: 2865912, 2017.
42. Dugan LL, You YH, Ali SS, Diamond-Stanic M, Miyamoto S, DeCleves AE, Andreyev A, Quach T, Ly S, Shekhtman G, *et al*: AMPK dysregulation promotes diabetes-related reduction of superoxide and mitochondrial function. J Clin Invest 123: 4888-4899, 2013.
43. Gu H, Zhong L, Zhang Y, Sun J, Liu L and Liu Z: Exploring the mechanism of Jinlida granules against type 2 diabetes mellitus by an integrative pharmacology strategy. Sci Rep 14: 10286, 2024.
44. Liu Y, Li Y, Xu L, Shi J, Yu X, Wang X, Li X, Jiang H, Yang T, Yin X, *et al*: Quercetin attenuates podocyte apoptosis of diabetic nephropathy through targeting EGFR signaling. Front Pharmacol 12: 792777, 2022.
45. He JY, Hong Q, Chen BX, Cui SY, Liu R, Cai GY, Guo J and Chen XM: Ginsenoside Rb1 alleviates diabetic kidney podocyte injury by inhibiting aldose reductase activity. Acta Pharmacol Sin 43: 342-353, 2022.
46. Li X, Wang J, Yan J, He JC, Li Y and Zhong Y: Additive renal protective effects between arctigenin and puerarin in diabetic kidney disease. Biomed Pharmacother 171: 116107, 2024.